Copper Tubing—Flexible 1/4-inch cooper tubing used to form the transmitting and receiving coils can be found at most hardware stores. The cost is approximately $1 per foot. The 55-gallon industrial plastic drums that the copper tubing was wrapped around can also be found at many hardware stores and costs approximately $70.

Miscellaneous—The WPT experiments also required 18-AWG magnet wire to form the transmitting and receiving loops, capacitors to set the resonant frequency of the loops, coaxial cables, and various rf connector adapters. All of these components can be purchased from Digi-Key Electronics (https://www.digikey.com/).

[a]Electronic mail: jake.bobowski@ubc.ca

[1]A. Kurs, A. Karalis, R. Moffatt, J. D. Joannopoulos, P. Fisher, and M. Soljačić, "Wireless power transfer via strongly coupled magnetic resonances," Science **317**(5834), 83–86 (2007).
[2]A. Karalis, J. D. Joannopoulos, and M. Soljačić, "Efficient wireless non-radiative mid-range energy transfer," Ann. Phys. **323**(1), 34–48 (2008).
[3]S. Y. R. Hui, W. Zhong, and C. K. Lee, "A critical review of recent progress in mid-range wireless power transfer," IEEE Trans. Power Electron. **29**(9), 4500–4511 (2014).
[4]S. Cheon, Y.-H. Kim, S.-Y. Kang, M. L. Lee, J.-M. Lee, and T. Zyung, "Circuit-model-based analysis of a wireless energy-transfer system via coupled magnetic resonances," IEEE Trans. Ind. Electron. **58**(7), 2906–2914 (2011).
[5]T. P. Duong and J.-W. Lee, "A dynamically adaptable impedance-matching system for midrange wireless power transfer with misalignment," Energies **8**(8), 7593–7617 (2015).
[6]The DG8SAQ VNWA 3 was designed by Prof. Thomas Baier from the Institute of Applied Natural Sciences of Hochschule Ulm. This instrument can be purchased online (https://www.sdr-kits.net/).
[7]M. J. Sibakoti and J. Hambleton, "Wireless power transmission using magnetic resonance," Cornell College (2011).
[8]E. F. Da Silva and M. K. McPhun, "Calibration techniques for one port measurement," Microwave J. **21**(6), 97–100 (1978); available at http://wrap.warwick.ac.uk/73386/" and "http://wrap.warwick.ac.uk/73386/1/WRAP_THESIS_Silva_1978.pdf.
[9]J. S. Bobowski and T. Johnson, "Permittivity measurements of biological samples by an open-ended coaxial line," Prog. Electromagn. Res. B **40**, 159–183 (2012).
[10]M. Mehdeizadeh, T. K. Ishii, J. S. Hyde, and W. Froncisz, "Loop-gap resonator: A lumped mode microwave resonant structure," IEEE Trans. Microwave Theory Tech. **31**(12), 1059–1064 (1983).
[11]Y. Liu and X. Zhang, "Metamaterials: A new frontier of science and technology," Chem. Soc. Rev. **40**, 2494–2507 (2011).
[12]J. Dubreuil, "Magnetic permeability at microwave frequencies measured using a toroidal split-ring resonator," Undergraduate thesis, University of British Columbia (2017).
[13]A. P. Sample, D. A. Meyer, and J. R. Smith, "Analysis, experimental results, and range adaptation of magnetically coupled resonators for wireless power transfer," IEEE Trans. Ind. Electron. **58**(2), 544–554 (2011).
[14]H. A. Jones, "A temperature scale for tungsten," Phys. Rev. **28**, 202–207 (1926).
[15]D. C. Agrawal, "The coiling factor in the tungsten filament lamps," Lat. Am. J. Phys. Educ. **5**(2), 443–449 (2011); avaiable at http://www.lajpe.org/june11/21_LAJPE_535_Agrawal_Plantilla_preprint_corr_f.pdf" and the url to page where the article is indexed is: "http://www.lajpe.org/index_june11.html#.
[16]A. Collado, S.-N. Daskalakis, K. Niotaki, R. Martinez, F. Bolos, and A. Georgiadis, "Rectifier design challenges for RF wireless power transfer and energy harvesting systems," Radioengineering **26**(2), 411–417 (2017).
[17]J. Dai and D. C. Ludois, "A survey of wireless power transfer and a critical comparison of inductive and capacitive coupling for small gap applications," IEEE Trans. Power Electron. **30**(11), 6017–6029 (2015).

Versatility of electrochemically grown dendrites in the undergraduate laboratory

S. Tuppan, D. Dams, Z. Olson, and W. J. Kim
Department of Physics, Seattle University, 901 12th Avenue, Seattle, Washington 98122

(Received 19 February 2018; accepted 15 May 2018)

We describe an experiment to fabricate atomic-scale contacts using electrochemically grown silver wires. The formation of a single-wire junction is directly observed and captured by an optical microscope, while electrical conductance of the wire, simultaneously recorded, is shown to be quantized. Further, a diffusion-limited aggregate (DLA) simulation is performed to compare the observed fractal formed by the silver dendrites. Our experiment directly exposes undergraduate students to exciting contemporary physics ranging from atomic-scale switches to fractal formation, all on a single experimental platform.
https://doi.org/10.1119/1.5040499

I. INTRODUCTION

One of the fascinating aspects of electron transport involving atomic-scale contact is the quantization of electrical conductance in units of $G_0 \equiv 2e^2/h$, where e is the electron's charge and h is Planck's constant. The wave-nature of electron is manifested as it moves through a narrow constriction whose size is comparable to its Fermi wavelength. A simple way to demonstrate this quantum of electrical conductance (i.e., quantized conductance) employs the so-called mechanical-break junction (MBJ), whereby a pair of metallic tips are repeatedly brought in and out of contact, while electrical conductance across the tips is measured. Distinct step-like conductance plateaus are readily observed, and histogram analysis reveals the quantized conductance up to several units of G_0.[1–4] Some MBJ setups have also been introduced as suitable undergraduate laboratory experiments or as demonstration apparatuses.[5–7]

Not only is the physics of atomic-scale electron transport interesting as a direct manifestation of the quantum effects on an ordinary object like a wire, but this area also provides opportunites to fabricate electronic devices at the minuscule size-level of single atoms and molecules. One notable effort to fabricate controllable atomic-scale contacts include the use of electrochemistry. Unlike the irreversible mechanical contacts made in the MBJ method, the electrochemical approach, by the processes of deposition and dissolution, can make the atomic-scale contacts *reversibly*, as demonstrated by several groups.[8,9] As a result, the use of electrochemistry for fabricating atomic-scale wires has gained much popularity over the last decade.[10,11]

In particular, Morpurgo *et al*. combined lithographic and electrochemical methods to produce "simple, controllable, reversible, and robust" junction fabrications on the order of 1 nm; their approach offers an exciting prospect of directly interfacing nano-scale structures to macroscopic devices.[12] But, there is another often overlooked by intrinsically interesting aspect of utilizing electrochemically grown wires as a means to fabricate atomic contacts-fractal formation by diffusion-limited aggregation (DLA), a model originally proposed by Witten and Sander in 1981.[14,15] Indeed, electrochemistry was one of the primary experimental tools used to investigate the metal-particle aggregation, as beautifully demonstrated with zinc and copper "leaves."[16–18]

Here, we report demonstration of quantized conductance across electrochemically grown silver (Ag) wires. With the aid of an optical microscope, optical images reveal a complex process of junction-crossing which involves random aggregation of Ag particles. We perform a DLA simulation on the random pattern formed by these particle aggregates and compare them with the observed images. The experimental component of our project makes its computational counterpart immediately relevant and provides an excellent platform to combine nanoscale physics involving electron transport measurements with one of the exciting computing techniques based on random walks.[19]

II. EXPERIMENTAL SETUP

Electrochemical growth is initiated inside a Teflon cell containing an electrolyte solution (0.1M HNO_3 + 0.01M $AgNO_3$). Above the Teflon cell is an optical microscope which enables us to capture images of the growth of Ag wires across the copper electrodes, as shown in top of Fig. 1. One of the copper electrodes is controlled by a motorized actuator (not shown); this actuator can move its attached electrode towards and away from the other electrode.

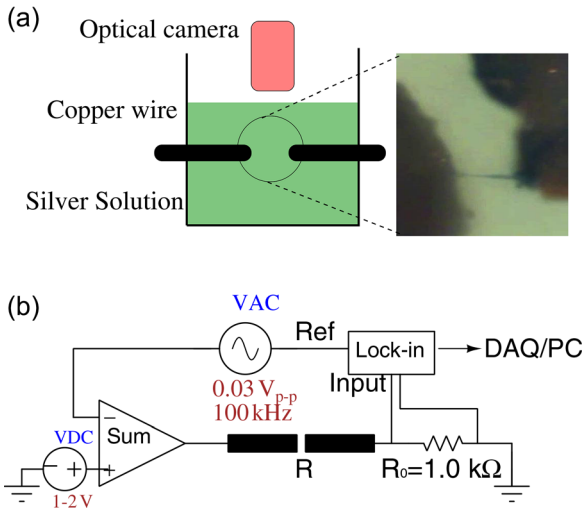

Fig. 1. Experimental (top) and electronic (bottom) setups: Electrochemical growth takes place between two copper electrodes (black) submerged in a silver solution inside a Teflon cell. Growth is driven by a dc source and is imaged by an optical microscope, while conductance measurements are simultaneously performed by a lock-in amplifier. The formation of a single Ag wire bridging the gap is visible on the top-right image captured by the optical scope. The gap between the electrodes is roughly 100 μm, and the width of the Ag wire is on the order of a few μm. On the electronic setup, a summing amplifier combines V_{dc}, a driving source of electrochemical growth and V_{ac} (≈ 30 mV), a reference signal from the lock-in amplifier. The lock-in output then directly measures a voltage across the 1-kΩ resistor, which is proportional to the total current through the junction.

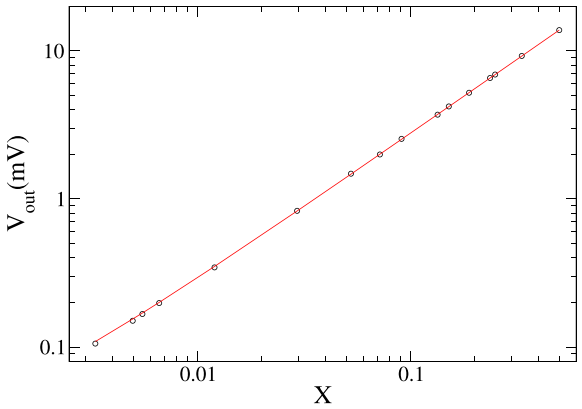

Fig. 2. Calibration result: The calibration is performed by placing a number of resistors of known resistance R between the copper electrodes. To linearize the relationship between V_{out} and R, we define $X \equiv (1 + R/R_0)^{-1}$, where $R_0 = 1.0\,\text{k}\Omega$. The measured data are fit to a straight line: $V_{out} = a + V_{ac}X$, where a represents an offset voltage. The best fit line gives: $V_{ac} = (28 \pm 2)$ mV and $a = (0.17 \pm 0.02)$ mV (Ref. 13). For the calibration, we used metal-film resistors (1% tolerance), with the resistance values ranging from 1 kΩ to 12.9 kΩ.

The Teflon cell was machined as a cylindrical shape with height $h = 2''$, and outer and inner diameters, $D = 5''$ and $d = 1.5''$, respectively. Located about one-third from the bottom is a pair of recessed holes ($d_s = 1/20''$) through which the copper electrodes are inserted from outside; these electrodes are sealed by rubber gaskets firmly pressed on the recessed holes to prevent leaks.

The electrochemical growth is driven by a dc-source $V_{dc} \approx 1$V, and the conductance measurements are facilitated by lock-in amplification, with an ac-source (rms) $V_{ac} = 30$ mV at 100 kHz. The physical distinction between the growth and conductance signals, as manifested by their frequencies and magnitudes, ensures that the crosstalk between them is minimized. The voltage V_{out}, measured across the reference resistor ($R_0 = 1\,\text{k}\Omega$), is directly proportional to the current through the junction: $I = V_{ac}/(R + R_0)$, where R represents the resistance of the *junction resistor*, i.e., the nanoscale wire created between the copper electrodes. Hence, the lock-in output voltage $V_{out} = V_{ac}/(1 + R/R_0)$ can be directly calibrated by placing a number of precision resistors of known resistances in the place of the junction resistor. The result is displayed in Fig. 2 for the fitted line $V_{out} = a + V_{ac}X$, where a represents an offset voltage. The conductance of the wire formed between the electrodes, which by definition is $G \equiv 1/R$, is found through the measured value of V_{out} using the following relations: $X = (V_{out} - a)/V_{ac}$ and $R = R_0(X^{-1} - 1)$. Throughout our discussions, we shall normalize the measured conductances in units of $G_0 = 1/(12.9\,\text{k}\Omega)$.

A. Experiment I: Demonstration of quantized conductance

Shown in Fig. 3 are results of conductance measurements that are recorded as the individual wire bridges the junction. In all of our runs, the growth voltage V_{dc} slowly ramps up to about $V_{dc}^{max} \approx 1.2$V until the conductance reaches a preset value, usually around $2G_0$ or $3G_0$, after which it ramps down. The growth could start off immediately at a constant voltage and terminate without ramping, but we chose to change V_{dc} gradually to ensure smooth growth, with a ramping speed of 2 mV/s.

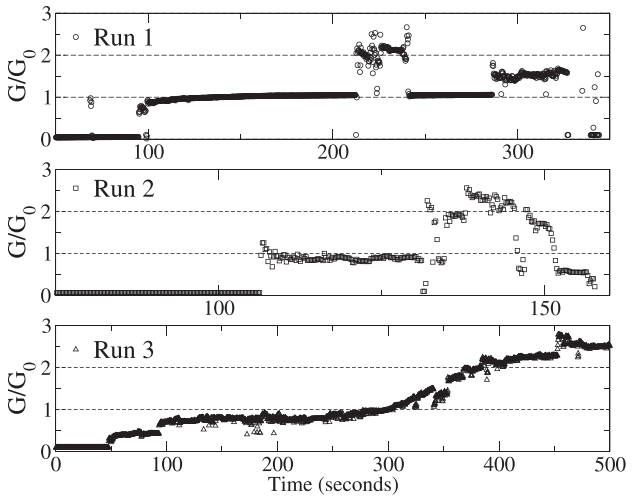

Fig. 3. Results of conductance measurements: The vertical axis is normalized in units of G_0. Quantized conductance at 1 G_0 is clearly visible and lasts over a hundred seconds in Run 1. There, a jump to $2G_0$ occurs briefly between 200 and 250 s and then the conductance decreases to $1\,G_0$ before increasing to a fractional step at $1.5G_0$. Similar steps are captured in Run 2, where a brief transition to $2.5G_0$ occurs. In Run 3, the conductance change is rather continuous, although the first conductance $1G_0$ appears robust (albeit slightly lower) and lasts over 200 s before gradually transiting to $2G_0$.

In Run 1, the quantized conductance at $1G_0$ is clearly observed and lasts over a hundred of seconds. It then briefly jumps to $2G_0$ and back down to $1G_0$ again. Around 300 s, it lands at a fractional conductance $1.5G_0$ for a few tens of seconds until it drops to the baseline. In Run 2, while the first conductance $1G_0$ is relatively stable, the second conductance is not; the fractional conductance at $2.5G_0$ is briefly captured before dropping down to half of $1G_0$. In contrast to the step-like changes observed in the other runs, Run 3 displays a *continuous* change in conductance while it shows a relatively stable, quantized step slightly below $1G_0$. The lower conductance is likely due to particle build-up on the electrode, which tends to increase the overall resistance, and hence lower conductance (see discussions below). A couple of remarks are in order with regard to our observations:

- The discrete conductance steps, as realized by our electrochemical setup, are remarkably long-lived—lasting over a few tens of seconds to over a hundred of seconds. In contrast, the atomic-scale contacts created by a typical mechanical-break junction (MBJ) apparatus have lifetime ranging from hundreds of micro-seconds and to a few mili-seconds,[1–3] though it is possible to fabricate more durable, MBJ-induced atomic-scale contacts in a controlled environment.[6] In our own undergraduate lab, students routinely observe quantized conductance of atomic-scale contacts created by the MBJ setup we previously constructed,[1] and the present electrochemical setup makes a great companion to the conventional MBJ apparatus.
- The baseline of conductance depends on the concentration of the nitric acid (HNO_3). The higher the concentration, the higher the baseline of conductance. For the measurements presented in Fig. 3, the baseline of conductance represents 3%–4% of G_0, above the zero-conductance line. To lower the conductance baseline, a few drops of distilled water can be added to dilute the overall concentration of the electrolyte solution.
- We ramped down the growth voltage V_{dc} once the conductance reached a preset value. The reason for this is to avoid excessive build-up of Ag aggregates that lead to a rapid rise to higher conductance without displaying quantized conductance, such as observed in Run 3. Notice that the wire will continue to grow during the ramp-down even though the rate of growth is continually decreased.
- The copper electrodes must maintain a minimum, gap-distance (typically, less than 100 μm) to create reliable single-wire contacts, as shown in Fig. 1. At a farther distance, the copper electrodes tend to accumulate Ag aggregates, and quantized conductance would become less pronounced. Even at a short gap-distance, repeated contacts make quantized conductance progressively harder to observe, which is further obscured by substantial build-up of Ag particles on the electrode itself. In that case, it was necessary to clean the electrodes and even to replace them entirely with a fresh pair of copper wires.
- As an alternative configuration in which to realize quantized conductance in an electrochemical environment, we point out the earlier work by Nakabayashi *et al*. who fabricated the atomic-scale contact by colliding 2D fractal on a circular ring, as opposed to our vertical configuration.[20] There, the fractal is observed to be grown *radially* outward from the center of the ring.

We observe that when the gap-distance between the copper electrodes widens, the single-wire crossing, such as captured in the inset of Fig. 1, becomes less frequent, and the contacting process is complicated by fractal formation as the Ag aggregates branch out to form multiple contacts (see our next discussion and additional images in the Appendix). As a result, this random branching significantly modifies the overall resistance across the junction and causes the measured conductance to be both non-integral and continuous as they build up. We believe that investigating this complex behavior of conductance change, impacted by the particle aggregates, is the beyond the scope of our present discussions. Instead, in what follows we present the experimental observations of fractal formation and compare them with computer simulations based on diffusion-limited aggregation.

B. Experiment II: Fractal observation and DLA simulation

The gap-distance between the electrodes is now increased to about 300 μm, and the electrochemical growth is initiated. For this experiment, one may forgo the lock-in measurements entirely and only apply the growth signal. As such, the present experiment is the simpler version of the original setup depicted in Fig. 1, only requiring a dc-power source and the relevant electrochemical preparation. The top of Fig. 4 shows progressive images demonstrating fractal formation—the process by which tree-like fractals begin to form on the bottom electrode and "branch" out towards the top electrode. The direct, real-time observation of the pattern formation of these fractals provides the students with an immediate experimental context from which to understand the underlying physical mechanism – diffusion-limited aggregation (DLA).

There is, however, a slight difference between our experimentally observed fractal and the conventional DLA discussed in the literature; instead of particles undergoing *pure* random walks, the Ag particles in our experiment tend to cluster "vertically" due to the greater gradient of electric potential

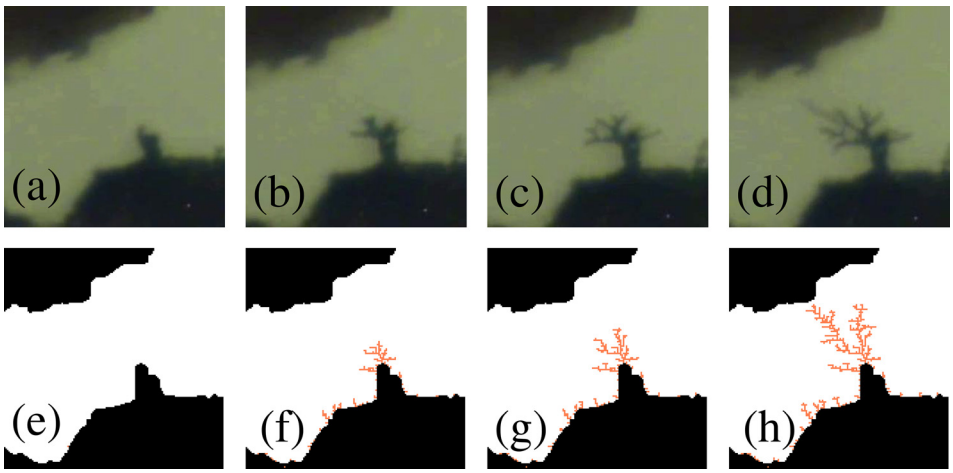

Fig. 4. Progressive images of bridging the junction by the DLA process: The top four images (a)–(d) are experimentally obtained, and the bottom four images (e)–(h) are computer-simulated. To account for the driving effect of electrostatic attraction, the particles are assigned with a higher probability of moving down than up (50% versus 10%), with equal probabilities for right and left directions (20%). For the experimentally obtained images, it takes about several minutes for a fractal to appear in full view, although the process could be expedited by applying a higher growth voltage at a shorter gap distance. Once the base site is raised to a certain level, such as the one shown in (a), the build-up accelerates. For instance, the time elapse between (c) and (d) is only a fraction of a second.

along that direction. This is because of the need of applying a constant electric potential ($V_{dc} \approx 1$ V) to sustain electrochemical growth of the wires. This externally established gradient will then favor the particles moving down towards the electrode, breaking the symmetry implied by pure random walks. Mathematically speaking, the general DLA problem can be formulated by the solution of Laplace's equation in which the electric potential at each site is directly proportional to the probability of a particle sticking to that particular site. For example, for pure random walks (i.e., in the absence of external potential), Laplace's equation is $\nabla^2 V = 0$ with zero potential around the lattice boundary. If Laplace's equation is solved numerically on the 2-D lattice, it satisfies the relation

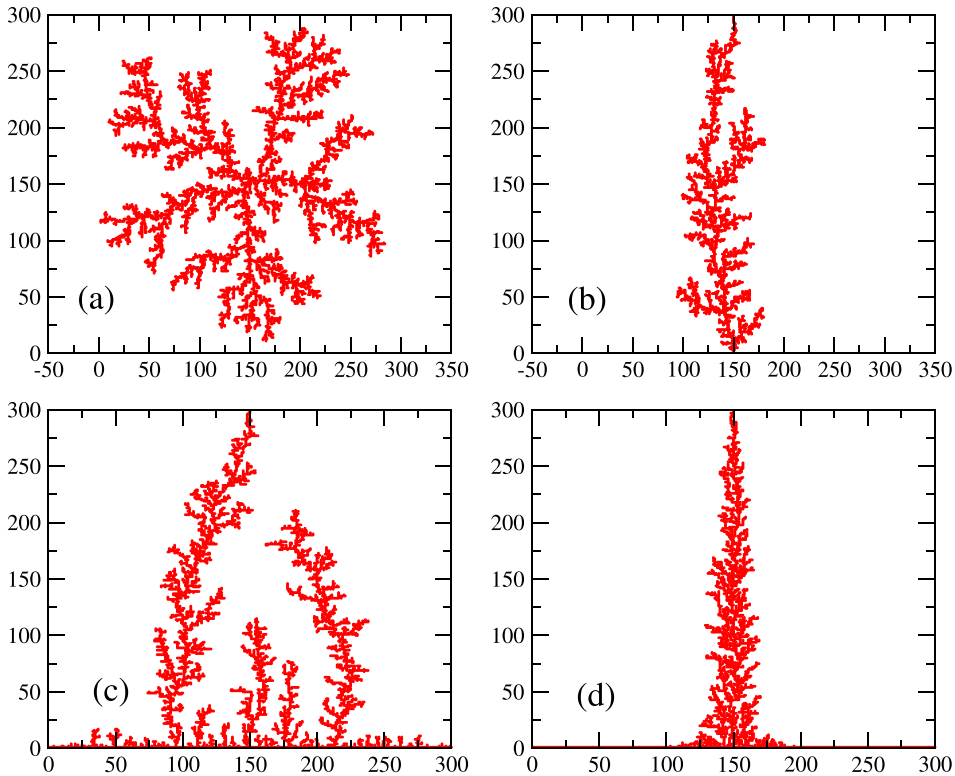

Fig. 5. Simulation results of diffusion-limited aggregates: (a) A seed site is at the center, and particles are introduced from a random point at the boundary; (b) a seed site is at the center of the bottom surface, and a particle is introduced from the center of the top surface for each iteration; (c) seed sites are along the bottom surface, and a particle is introduced from the center of the top surface for each iteration. For images (a)–(c), the particles perform a random walk with an equal probability in all four directions. That is, the equal probability of 25% for top, down, left, and right steps; (d) Same conditions as described in (c), but with the higher probability of moving down than in other directions. In this case, we have 8%, 60%, 16%, and 16% for the probabilities of moving in top, bottom, left, and right direction, respectively. All simulations are performed on a square lattice of 300 sites.

$$V(i,j) = \frac{1}{4}[V(i+1,j) + V(i-1,j) + V(i,j+1) + V(i,j-1)], \quad (1)$$

where (i, j) represents the specific lattice site where the potential is being evaluated. As seen from Eq. (1), $V(i, j)$ is the average of the potential of the four neighboring sites—the main result from the finite difference method for solving the 2D boundary value problems. Because the potential at the boundary is zero, V is also zero everywhere on the lattice. Thus, the pure random walk gives equal probabilities in all four directions (25% for each). On the other hand, the potential difference established between the top and the bottom electrodes in our experiment gives rise to a higher probability of the particle moving down than that of moving up, with roughly equal probabilities in lateral movement. The bottom of Fig. 4 is the result of our computer simulation taking into account the asymmetric probabilities in random walks.

The DLA simulation itself may be done as an independent project, aided by a standard textbook on computer simulation like the one written by Gould and Tobochnik.[19] Students are encouraged to use a programming language of their own choice, such as MATLAB, PYTHON, or C#. The computer simulation is performed as follows: A seed particle is placed in the middle of a square lattice, for example, at (150,150), as initiated in Fig. 5(a). A random-walk particle is introduced from a distant site near the lattice boundary; the particle will either escape to "infinity" (outside the boundary) or stick, irreversibly, to a neighboring site of the seed. Now introduce another particle, which again either escapes to infinity or sticks to one of the neighboring sites of the two-particle cluster. The process repeats until the tip of the cluster reaches at the lattice boundary. Figure 5 shows several examples of aggregates of a few thousand particles on a square lattice under different conditions (e.g., varying seeding and emerging sites as well as the step probabilities).

Note that our DLA simulation uses a set of fixed probabilities to facilitate each random walk at a given site. To make the simulation more realistic, one could consider adding a subroutine program in which the new boundary-value problem is solved each time a new particle is attached to the existing cluster, thereby updating the probabilities for all sites for each iteration. The interested reader is encouraged to explore this feature as an add-on program, although we believe that doing so will substantially increase computing time without effecting much change on the final image generated by the fixed-probability simulation, as performed in the present report.[22]

The entire experiment including construction of the electrochemical cell and lock-in calibration was undertaken by two undergraduate students during an 8-week period of summer research. A third student developed the DLA simulation in the following summer. Apart from the lock-in amplifier, the only major piece of equipment required to record fractal images is an optical microscope, which we purchased as used (<$500). The DLA simulation was performed on the same laboratory computer that interfaced the conductance measurements via a DAQ card (<$500). Other materials include common resistors, copper wires, and some standard chemical solutions.

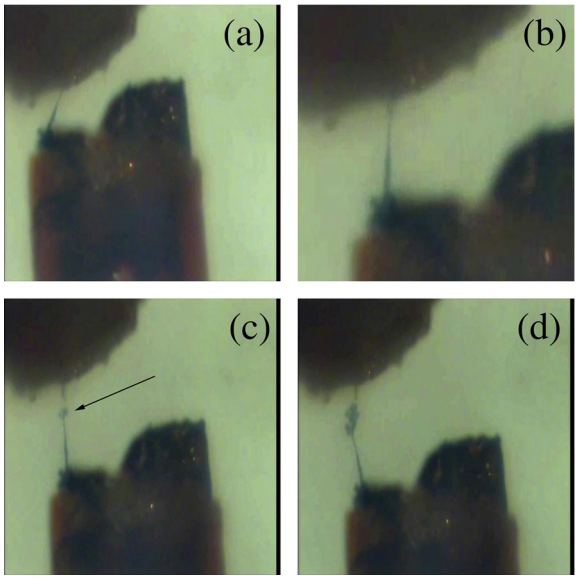

Fig. 6. Fractal emerging at the tip of a broken wire: (a) We first fabricate a single-wire junction between the two electrodes, and then (b) stretch it by retracting the bottom electrode. (c) The wire breaks about one-third way from top, as indicated by an arrow and (d) fractal growth begins.

III. CONCLUSIONS

We have demonstrated the versatility of electrochemically grown Ag wires in the undergraduate laboratory. Atomic-scale contacts can be fabricated by growing these wires between a pair of electrodes. Our *in-situ* optical images reveal a fascinating process of fractal formation, driven by diffusion-limited aggregation. A DLA simulation is also performed to compare with the experimentally observed fractals. Our experiment utilizing electrochemistry provides students with

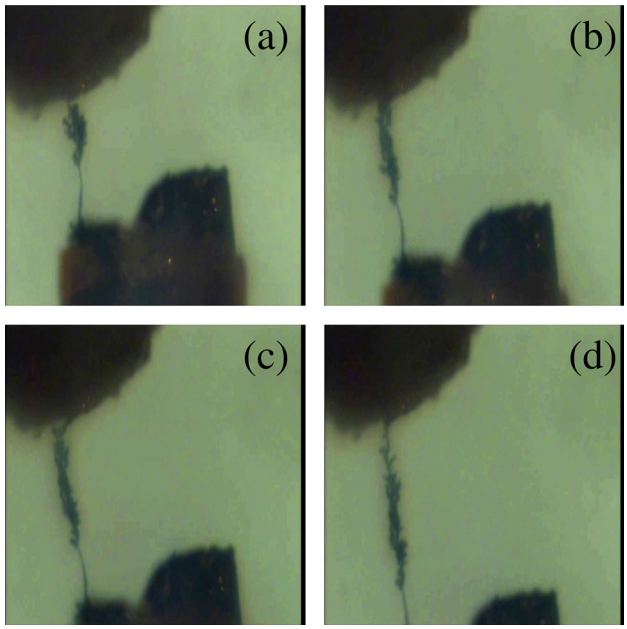

Fig. 7. Growing a fractal vertically: (a) We begin with a fractal atop a wire anchored to the bottom electrode. (b) As the fractal grows, the bottom electrode is retracted to maintain a short gap (not visible in the figure) between the fractal "head" and the top electrode. Due to the head-electrode proximity, an immediate, vertical build-up follows (b). The bottom electrode is then further retracted, and the vertical buildup continues in (c) and (d). The final image resembles the simulation result depicted in Fig. 5(d) in which the highest probability is assigned for particles moving down (hence the apparent vertical growth). Clearly, the short separation between the seed site (i.e., the wire) and the source site (i.e., the top electrode) preferentially promotes the vertical growth.

an excellent opportunity to explore contemporary topics in physics ranging from atomic-scale electron transport to fractal formation, all on a single experimental platform.

APPENDIX: ADDITIONAL IMAGES CAPTURING FRACTAL GROWTH

Here we present two sets of additional micrographs (Figs. 6 and 7) we obtained during our fractal growth.

[1]C. Rackson, A. Watt, and W. J. Kim, "Effect of surface contact potential in atomic-size contacts," Phys. Lett. A **379**, 2239–2244 (2015).
[2]J. L. Costa-Krämer, N. García, P. Garca-Mochales, and P. A. Serena, "Nanowire formation in macroscopic metallic contacts: quantum mechanical conductance tapping a table top," Surf. Sci. Lett. **342**, L1144–L1149 (1995).
[3]J. L. Costa-Krämer, N. García, and H. Olin, "Conductance quantization histograms of gold nanowires at 4 K," Phys. Rev. B **55**, 12910–12913 (1997).
[4]D. L. Bakker, Y. Noat, A. I. Yanson, and J. M. van Ruitenbeek, "Effect of disorder on the conductance of a Cu atomic point contact," Phys. Rev. B **65**, 235416 (2002).
[5]E. L. Foley, D. Candela, K. M. Martini, and M. T. Tuominen, "An undergraduate laboratory experiment on quantized conductance in nanocontacts," Am. J. Phys. **67**, 389–393 (1999).
[6]E. H. Huisman, F. L. Bakker, J. P. van der Pal, R. M. de Jonge, and C. H. van der Wal, "Public exhibit for demonstrating the quantum of electrical conductance," Am. J. Phys. **79**, 856–860 (2011).
[7]R. Tolley, A. Silvidi, C. Little, and K. F. Eid, "Conductance quantization: A laboratory experiment in a senior-level nanoscale science and technology course," Am. J. Phys. **81**, 14–19 (2013).
[8]C. Z. Li and N. J. Tao, "Quantum transport in metallic nanowires fabricated by electrochemical deposition/dissolution," Appl. Phys. Lett. **72**, 894–896 (1998).
[9]M. Akai-Kasaya, K. Nishihara, A. Saito, Y. Kuwahara, and M. Aono, "Quantum point-contact switches using silver particles," Appl. Phys. Lett. **88**, 023107 (2006).
[10]N. Tao "Electrochemical fabrication of metallic quantum wires," J. Chem. Edu. **82**, 720–726 (2005).
[11]M. R. Calvo, A. I. Mares, V. Climent, J. M. van Ruitenbeek, and C. Untiedt, "Formation of atomic-sized contacts controlled by electrochemical methods," Phys. Stat. Sol. **204**, 1677–1685 (2007).
[12]A. F. Morpurgo, C. M. Marcus, and D. B. Robinson, "Controlled fabrication of metallic electrodes with atomic separation," Appl. Phys. Lett. **74**, 2084–2086 (1999).
[13]In principle, the intercept a should be zero as the junction resistance approaches infinity and hence X approaches zero. But, in our by calibration, the largest value of resistance used was $R_{max} = 12.9\,k\Omega$, and this rather small R_{max} may have caused a deviation from the zero-intercept, as evidenced by the finite value of the offset parameter ($170\,\mu V$). Alternatively, we suspect that the non-zero intercept reflects a small amount of electronic pickup at 100 kHz in the open circuit (i.e., no resistor connected across the electrode).
[14]T. A. Witten, Jr. and L. M. Sander, "Diffusion-limited aggregation, a kinetic critical phenomenon," Phys. Rev. Lett. **47**, 1400–1403 (1981).
[15]T. C. Halsey, "Diffusion-limited aggregation: A model for pattern formation," Phys. Today **53**(11), 36–41 (2000).
[16]M. Matsushita, M. Sano, Y. Hayakawa, H. Honjo, and Y. Sawada, "Fractal structures of zinc metal leaves grown by electrodeposition," Phys. Rev. Lett. **53**, 286–289 (1984).
[17]D. Barkey, F. Oberholtzer, and Q. Wu, "Kinematic anisotropy and dendritic growth in electrochemical deposition," Phys. Rev. Lett. **75**, 2980 (1995).
[18]H. Hahn, R. Krupke, F. Schramm, T. Scherer, B. Dinga, and X. Song, "Silver nanowires growth via branch fragmentation of electrochemically grown silver dendrites," Chem. Commun. **0**, 1130–1132 (2009).
[19]H. Gould and J. Tobochnik, *An Introduction to Computer Simulation Methods*, 2nd ed. (Addison-Wesley Publishing Company, CA, 1996), p. 477.
[20]S. Nakabayashi, H. Sakaguchi, R. Baba, and E. Fukushima, "Quantum contact by colliding 2D fractal," Nano Lett. **1**, 507–510 (2001).
[21]A. Wlasenko, F. Soltani, D. Zakopcan, D. Sinton, and G. M. Steeves, "Diffusion-limited and advection-driven electrodeposition in a microfluidic channel," Phys. Rev. E **81**, 021601 (2010).
[22]As another driving mechanism, advection can be also introduced. See the article by A. Wlasenko *et al*. (Ref. 21).